highest thermal displacements of this species occur along directions perpendicular to the proposed direction of motion, approximately towards the neighboring partially occupied site.

We are indebted to Dr Peter Höhn of the Max-Planck-Institut für Festkörperforschung for providing single-crystal intensity data and to Eva-Marie Peters for assistance with the structure determination. We thank Mike Jercinovic of the Massachusetts Institute for Technology for supplying microprobe analyses and Ortrud Buresch of the Max-Planck-Institut für Festkörperforschung for performing the plasma spectroscopy. SH is grateful to the AT&T Cooperative Fellowship Program, the Fulbright Foundation and the Alexander von Humboldt Foundation for providing financial support at various stages of this research.

References

FROSTÄNG, S., GRINS, J. & NYGREN, M. (1988). *Chem. Scr.* **28**, 107–110.
GOODENOUGH, J. B., HONG, H. Y.-P. & KAFALAS, J. A. (1976). *Mat. Res. Bull.* **11**, 203–220.
GUNAWARDANE, R. P., HOWIE, R. A. & GLASSER, F. P. (1982). *Acta Cryst.* B**38**, 1405–1408.
HAILE, S. M. (1992). PhD thesis. Massachusetts Institute of Technology, Cambridge, Massachusetts, USA.
HAILE, S. M., SIEGRIST, T., LAUDISE, R. A. & WUENSCH, B. J. (1991). *Mat. Res. Soc. Symp. Proc.* **210**, 645–651.
HAILE, S. M., WUENSCH, B. J. & LAUDISE, R. A. (1993). *J. Cryst. Growth*, **131**, 373–386.
HAILE, S. M., WUENSCH, B. J., SIEGRIST, T. & LAUDISE, R. A. (1992). *Solid State Ionics*, **53–56**, 1292–1301.
HAILE, S. M., WUENSCH, B. J., SIEGRIST, T. & LAUDISE, R. A. (1993). *J. Cryst. Growth*, **131**, 352–372.
LAUDISE, R. A. (1987). In *Advanced Crystal Growth*, edited by P. M. DRYBURGH, B. COCKAYNE & K. G. BARRACLOUGH. New York: Prentice Hall.
LIEBAU, F. (1985). *Structural Chemistry of Silicates: Structure, Bonding, and Classification*. Berlin: Springer-Verlag.
PUSHCHAROVSKII, D. Y., KARPOV, O. G., POBEDIMSKAYA, E. A. & BELOV, N. V (1977). *Sov. Phys. Dokl.* **22**, 292–293.
SCHAMBER, F., WODKE, N. & MCCARTHY, J. (1981). *ZAF Matrix Correction Procedure for Bulk Samples: Operation and Program Description*, 31pp. Tracor Northern Publication TN-2120, Middleton, Wisconsin, USA.
SHANNON, R. D. & PREWITT, C. T. (1969). *Acta Cryst.* B**25**, 925–946.
SHANNON, R. D., TAYLOR, B. E., GIER, T. E., CHEN, H.-Y. & BERZINS, T. (1978). *Inorg. Chem.* **17**, 958–964.
SHELDRICK, G. M. (1985). *Crystallographic Computing* 3, edited by G. M. SHELDRICK, C. KRÜGER & R. GODDARD, pp. 175–189. Oxford Univ. Press.
SMOLIN, Y. I. (1970). *Sov. Phys. Crystallogr.* **15**, 23–27.
TUTTLE, O. F. (1949). *Geol. Soc. Am. Bull.* **60**, 1927.
WATANABE, M. & WUENSCH, B. J. (1993). *J. Solid State Chem.* In the press.

Acta Cryst. (1995). B**51**, 680–687

Structure of $Cs_3(HSO_4)_2(H_2PO_4)$ – a New Compound with a Superprotonic Phase Transition

BY S. M. HAILE

Department of Materials Science and Engineering, Box 352120, *University of Washington, Seattle, WA* 98195, *USA*

AND K.-D. KREUER AND J. MAIER

Max-Planck-Institut für Festkörperforschung, 70569 *Stuttgart, Heisenbergstrasse* 1, *Germany*

(*Received* 15 *February* 1995; *accepted* 27 *April* 1995)

Abstract

Solid-solution studies in the $CsHSO_4$–CsH_2PO_4 system carried out in a search for low-temperature proton conducting materials yielded the new compound $Cs_3(HSO_4)_2(H_2PO_4)$ [tricesium bis(hydrogensulfate) dihydrogenphosphate]. Single-crystal X-ray measurements (performed at room temperature) revealed that $Cs_3(HSO_4)_2(H_2PO_4)$ crystallizes in space group $P2_1/n$ and has lattice parameters a = 19.546 (3), b = 7.8798 (10), c = 9.1854 (17) Å and β = 100.536 (14)°. With four formula units in the unit cell, and a cell volume of 1390.7 (4) Å^3, $Cs_3(HSO_4)_2(H_2PO_4)$ has a calculated density of 3.295 Mg m^{-3}. 18 non-H atoms were located in the asymmetric unit. Refinement using anisotropic temperature factors for all 18 non-H atoms yielded weighted residuals based on F^2 and F values, respectively, of 9.32 and 4.56% for all observed reflections. Hydrogen sites were identified (but not refined) on the basis of geometric considerations. The structure contains zigzag chains of hydrogen-bonded anion tetrahedra that are, in turn, bonded to one another to form a three-dimensional structure. In the temperature range 381–398 K the compound transforms into a structure which is rhombohedral, pseudo-body-centered cubic, with lattice constants a = 6.95 (2) Å and $\alpha \simeq 90°$.

Introduction

Many classes of solid acid sulfates and selenates are known to undergo superprotonic phase transitions

at elevated temperatures. These include $MHXO_4$ [Baranov, Fedosyuk, Schagina (*sic*) & Shuvalov, 1984], $M_5H_3(XO_4)_4.H_2O$ [M = Se, Rb, NH_4, K; X = S, Se (Merinov, Baranov, Shuvalov & Shchagina, 1991*a*,*b*)], $M_3H(SeO_4)_2$ (Pawlowski, Pawlaczyk & Hilczer, 1990) and $(NH_4)_4H_2(SeO_4)_3$ (Pawlaczyk, Salman, Pawlowski, Czapla & Pietraszko, 1986) and the corresponding deuterated analogs. We recently reported the presence of a similar transition in $Cs_3(HSO_4)_2(H_2PO_4)$ (Haile, Lentz, Kreuer & Maier, 1995), thereby introducing a new compound, and perhaps a new class of compounds, which belong in the broad family of low-temperature proton conductors. We describe here in detail the room-temperature structure of this material and discuss briefly the transitions the compound undergoes.

Experimental

Crystal growth and characterization

Crystals of $Cs_3(HSO_4)_2(H_2PO_4)$ were grown by evaporation from aqueous solution. Cesium carbonate was placed in a 60:40 solution of absolute H_2SO_4 and H_3PO_4. To this, just enough water was added to cause dissolution. Upon maintaining the solution at a temperature of approximately 288 K, large crystals, 1 × 2 × 5 mm, formed after 5–10 days. The composition of the crystals was determined *via* electron microprobe measurements and by inductively coupled plasma (ICP) spectroscopy after dissolution and dilution in water. Samples for microprobe analysis were cut to expose the interior and both this area and the exterior were examined for compositional variations

Under the growth conditions described above, a small amount of Cs_2SO_4 coprecipitated within the $Cs_2(HSO_4)_2(H_2PO_4)$ crystals. This was evident from the microprobe measurements, in which regions showing either a 2:1 ratio of sulfur to phosphorus or no phosphorus at all were observed. ICP spectroscopy, which samples larger volumes of material than microprobe analysis, gave less pronounced, but nonetheless significant, variations in the measured composition. In addition to the salt coprecipitate, $Cs_3(HSO_4)_2(H_2PO_4)$ crystals often contained small voids, occasionally filled with liquid.

Phase transitions

Both thermal decomposition and structural phase transitions were studied in $Cs_3(HSO_4)_2(H_2PO_4)$. The former was investigated using thermal gravimetric analysis (Netzsch balance, STA model 429). Samples were heated under vacuum, and evolved gases were examined *via* mass spectrometry (Balzers QMG511). Structural phase transitions were investigated using differential scanning calorimetry (Dupont DSC 7), performed under flowing argon and using high-temperature X-ray powder diffraction. The diffraction experiments were conducted with a Guinier camera equipped with a moving cassette (Simon, 1971). The pattern obtained on film was converted to digitized data using a 600 d.p.i. scanner. Raw intensities were corrected for film sensitivity using silicon as a standard.

Intensity data collection and refinement

Single-crystal X-ray intensity data were collected at room temperature from an as-synthesized specimen measuring 0.02 × 0.06 × 0.1 mm^3 in size. Data were obtained in Mo $K\alpha$ radiation (λ = 0.71073 Å) using a Siemens *R3v/m* diffractometer. Refinement of the lattice parameters, using the locations of 23 peaks, revealed $Cs_3(HSO_4)_2(H_2PO_4)$ to be monoclinic with lattice parameters a = 19.546 (3), b = 7.8798 (10), c = 9.1854 (17) Å and β = 100.536 (14)°. The remaining data collection parameters, along with some crystallographic data and parameters related to the refinement, are provided in Table 1.

We solved the structure by first locating the Cs, S and P atoms by direct methods, and subsequently the O atoms from a Fourier difference map. Direct methods calculations were performed using the *SHELXS*86 program (Sheldrick, 1985); Fourier synthesis calculations were conducted using the *SHELXL*93 program (Sheldrick, 1992). H-atoms positions were identified on the basis of geometric considerations, as discussed below, but were not entered into Fourier calculations. The final weighted residuals, after employing anisotropic thermal parameters for all (non-H) atoms and an overall extinction correction, were 9.32 and 4.56%, as calculated for F^2 and F, respectively. Refinement was carried out by minimizing $R(F^2) = \Sigma w|(F_{obs})^2 - (F_{calc})^2|$ values (as per the *SHELXL* program); the value of the latter residual, $R(F)$, is provided merely for comparison with literature R values, typically derived from refinements on F. Calculated and observed F^2 have been deposited.*

Discussion of structure

Atomic coordinates and isotropic thermal parameters for the 18 non-H atoms in the asymmetric unit are reported in Table 2. A thermal ellipsoid representation of the structure is shown in Fig. 1. The cation ellipsoids are fairly spherical, and the oxygen ellipsoids show the thermal vibrations to be restrained to directions perpendicular to the X—O bond, as expected.

Polyhedral coordination and connectivity

Interatomic distances in the cation coordination polyhedra are reported in Table 3. The three crystallograph-

* A list of structure factors has been deposited with the IUCr (Reference: DU0399). Copies may be obtained through The Managing Editor, International Union of Crystallography, 5 Abbey Square, Chester CH1 2HU, England.

Table 1. *Experimental details*

Crystal data	
Chemical formula	$Cs_3(HSO_4)_2(H_2PO_4)$
Chemical formula weight	689.85
Cell setting	Monoclinic
Space group	$P2_1/n$
a (Å)	19.546 (3)
b (Å)	7.8798 (10)
c (Å)	9.1854 (17)
β (°)	100.536 (14)
V (Å^3)	1390.7 (4)
Z	4
D_x (Mg m^{-3})	3.295
Radiation type	Mo $K\alpha$
Wavelength (Å)	0.71073
No. of reflections for cell parameters	23
θ range (°)	4–55
μ (mm^{-1})	7.788
Temperature (K)	298
Crystal form	Irregular
Crystal size (mm)	0.02 × 0.06 × 0.1
Crystal color	Colorless
Data collection	
Diffractometer	Siemens $R3v/m$
Data collection method	Wyckoff
Absorption correction	Ψ scan
No. of measured reflections	3268
No. of independent reflections	3184
No. of observed reflections	3161
Criterion for observed reflections	$I > -2\sigma(I)$
R_{int}	0.0514
θ_{max} (°)	55.04
Range of h, k, l	$0 \rightarrow h \rightarrow 25$ $0 \rightarrow k \rightarrow 10$ $-11 \rightarrow l \rightarrow 11$
Refinement	
Refinement on	F^2
$R[F^2 > 2\sigma(F^2)]$	0.0833
$wR(F^2)$	0.0932
S	1.059
No. of reflections used in refinement	3161
No. of parameters used	164
H-atom treatment	Not refined
Weighting scheme	$w = [\sigma^2F_o^2 + 0.0516P^2 + 1.7824P]^{-1}$, where $P = 1/3(F_o^2 - 2F_c^2)$
$(\Delta/\sigma)_{max}$	0.226
$\Delta\rho_{max}$(e Å^{-3})	1.174
$\Delta\rho_{min}$(e Å^{-3})	−1.184
Extinction correction method	F_c = scale factor $[1 + 0.001\chi F_c^2(\lambda^3/\sin 2\theta)]^{-1/4}$
Extinction coefficient	0.00133 (12)
Source of atomic scattering factors	Cromer & Waber (1974)
Computer programs	
Structure solution	*SHELXS* (Sheldrick, 1985)
Structure refinement	*SHELXL* (Sheldrick, 1992)
Molecular graphics	Fig. 1 by *ORTEP* (Johnson, 1971) and Figs. 2(*a*), 3 and 4 using *ATOMS* from Shape Software
Powder analysis	*JADE* Software from MDI

ically independent Cs atoms are coordinated by 11, 10 and 10 O atoms, respectively. The observed coordination numbers and average Cs—O distance, 3.28 (17) Å, are consistent with typical values for Cs (Shannon & Prewitt, 1969).

Table 2. *Fractional atomic coordinates and equivalent isotropic displacement parameters* (Å^2)

$U_{eq} = (1/3)\sum_i\sum_j U_{ij}a_i^*a_j^*\mathbf{a}_i.\mathbf{a}_j.$

	x	y	z	U_{eq}
Cs(1)	0.31893 (2)	0.13498 (5)	0.40528 (4)	0.03998 (13)
Cs(2)	0.32727 (2)	−0.14553 (4)	0.86607 (4)	0.03707 (13)
Cs(3)	0.49681 (2)	0.40789 (5)	0.25988 (4)	0.03644 (12)
S(1)	0.16309 (7)	0.1405 (2)	0.06215 (15)	0.0307 (3)
S(2)	0.15817 (7)	−0.1324 (2)	0.5803 (2)	0.0326 (3)
P	0.49237 (7)	−0.0815 (2)	0.24896 (13)	0.0268 (3)
O(1)	0.5171 (2)	0.0287 (5)	0.1330 (4)	0.0349 (8)
O(2)	0.2181 (2)	−0.0206 (5)	0.5972 (5)	0.0484 (11)
O(3)	0.4315 (2)	−0.1928 (6)	0.1744 (4)	0.0431 (10)
O(4)	0.4473 (2)	0.1993 (5)	0.6777 (4)	0.0416 (9)
O(5)	0.4714 (2)	0.0264 (5)	0.3710 (4)	0.0321 (8)
O(6)	0.1596 (3)	−0.2471 (6)	0.4457 (5)	0.0517 (11)
O(7)	0.1644 (2)	−0.2446 (6)	0.7110 (5)	0.0439 (10)
O(8)	0.1719 (2)	0.2376 (6)	0.2065 (5)	0.0432 (10)
O(9)	0.0927 (2)	−0.0419 (6)	0.5520 (5)	0.0519 (12)
O(10)	0.6420 (3)	0.2411 (6)	0.4411 (5)	0.0505 (11)
O(11)	0.2337 (2)	0.0701 (6)	0.0571 (5)	0.0488 (11)
O(12)	0.6141 (2)	0.4963 (6)	0.5598 (5)	0.0486 (11)

Table 3. *Coordination polyhedra in* $Cs_3(HSO_4)_2(H_2PO_4)$; *bond distances* (Å) *and angles* (°)

Number in parentheses after atom identifies atom in terms of Table 2; numbers in parentheses after distance indicate the standard deviation in the last digit(s).

(*a*) Cesium polyhedra

Cs(1)—O(2)	3.125 (4)	Cs(2)—O(3^{vii})	3.194 (4)
Cs(1)—O(5)	3.170 (4)	Cs(2)—O(11^{vii})	3.237 (4)
Cs(1)—O(12^{i})	3.179 (5)	Cs(2)—O(7^{v})	3.248 (5)
Cs(1)—O(8)	3.214 (4)	Cs(2)—O(7)	3.333 (4)
Cs(1)—O(4)	3.243 (4)	Cs(2)—O(9^{vi})	3.512 (5)
Cs(1)—O(8^{ii})	3.311 (5)	Cs(2)—O(6^{v})	3.571 (5)
Cs(1)—O(10^{iii})	3.311 (5)	Average	3.26 (17)
Cs(1)—O(11)	3.364 (5)	Cs(3)—O(12^{i})	3.054 (4)
Cs(1)—O(6^{iv})	3.454 (4)	Cs(3)—O(9^{viii})	3.095 (4)
Cs(1)—O(7^{v})	3.607 (4)	Cs(3)—O(9^{iv})	3.097 (5)
Cs(1)—O(11^{iv})	3.615 (5)	Cs(3)—O(5)	3.242 (4)
Average	3.33 (17)	Cs(3)—O(1)	3.257 (4)
Cs(2)—O(10^{iii})	3.084 (4)	Cs(3)—O(10)	3.289 (5)
Cs(2)—O(2)	3.114 (5)	Cs(3)—O(4^{i})	3.298 (4)
Cs(2)—O(2^{vi})	3.122 (5)	Cs(3)—O(12)	3.320 (5)
Cs(2)—O(1^{iii})	3.176 (4)	Cs(3)—O(3^{ix})	3.432 (5)
		Cs(3)—O(6^{iv})	3.506 (5)
		Average	3.26 (15)

(*b*) XO_4 tetrahedra

S(1)—O(12^{x})	1.440 (4)	S(2)—O(6)	1.535 (4)
S(1)—O(10^{x})	1.452 (4)	Average	1.48 (4)
S(1)—O(11)	1.497 (4)	P—O(1)	1.521 (4)
S(1)—O(8)	1.513 (4)	P—O(5)	1.522 (3)
Average	1.48 (4)	P—O(3)	1.534 (4)
S(2)—O(9)	1.446 (4)	P—O(4^{iii})	1.554 (4)
S(2)—O(2)	1.451 (4)	Average	1.53 (2)
S(2)—O(7)	1.478 (4)		

O(10)—S(1)—O(12)	111.99 (29)	O(7)—S(2)—O(2)	109.32 (27)
O(11)—S(1)—O(12)	109.68 (27)	O(6)—S(2)—O(2)	108.08 (28)
O(8)—S(1)—O(12)	111.11 (26)	O(6)—S(2)—O(7)	106.90 (28)
O(11)—S(1)—O(10)	110.44 (28)	O(5)—P—O(1)	111.09 (23)
O(8)—S(1)—O(10)	108.49 (27)	O(3)—P—O(1)	109.52 (22)
O(8)—S(1)—O(11)	104.90 (25)	O(4)—P—O(1)	109.34 (23)
O(2)—S(2)—O(9)	112.97 (30)	O(3)—P—O(5)	110.89 (23)
O(7)—S(2)—O(9)	112.34 (27)	O(4)—P—O(5)	107.44 (22)
O(6)—S(2)—O(9)	106.93 (27)	O(4)—P—O(3)	108.48 (28)

Symmetry codes: (i) $-x+1, -y+1, -z+1$; (ii) $-x+\frac{1}{2}, y-\frac{1}{2}, -z+\frac{1}{2}$; (iii) $-x+1, -y, -z+1$; (iv) $-x+\frac{1}{2}, y+\frac{1}{2}, -z+\frac{1}{2}$; (v) $-x+\frac{1}{2}, y+\frac{1}{2}, -z+\frac{3}{2}$; (vi) $-x+\frac{1}{2}, y-\frac{1}{2}, -z+\frac{3}{2}$; (vii) $x, y, z+1$; (viii) $x+\frac{1}{2}, -y+\frac{1}{2}, z-\frac{1}{2}$; (ix) $x, y+1, z$; (x) $x-\frac{1}{2}, -y+\frac{1}{2}, z-\frac{1}{2}$.

Table 4. *Potential* H-*atom positions as determined from an optimization of* X—O—H *angles and* $X\cdots$H *distances*

Oxygen nearest neighbors, the distance between nearest neighbors and the hydrogen site symmetry are also given.

	x	y	z	O neighbors	d(O···O) (Å)	Site symmetry
H(1)	0.448	0.200	0.676	O(4)—O(7^{i})	2.613 (6)	1
H(2)	0.204	−0.310	0.460	O(6)—O(11^{ii})	2.539 (7)	1
H(3)	0.397	−0.203	0.241	O(3)—O(8^{ii})	2.528 (6)	$\bar{1}$
H(4)*($K=\frac{1}{2}$)	0.498	−0.015	0.039	O(1)—O(1^{iii})	2.454 (7)	$\bar{1}$
H(5)*($K=\frac{1}{2}$)	0.219	0.0545	0.683	O(5)—O(5^{iv})	2.464 (7)	$\bar{1}$

Symmetry codes: (i) $-x+\frac{1}{2}, y+\frac{1}{2}, -z+\frac{3}{2}$; (ii) $-x+\frac{1}{2}, y-\frac{1}{2}, -z+\frac{1}{2}$; (iii) $-x+1, -y, -z$; (iv) $-x+1, -y, -z+1$.

In the initial stages of the structure determination, three crystallographically independent XO_4 sites were quickly located. However, the central X ion (either S^{5+} or P^{6+}) could not be identified merely on the basis of Fourier calculations, because of the presence of the strong scatterer Cs. For this same reason, protons could not be located from Fourier difference maps. Consequently, the structure determination was completed using the following crystal-chemical arguments.

A comparison of O···O distances in $Cs_3(HSO_4)_2(H_2PO_4)$ shows that there are five intertetrahedral oxygen–oxygen distances that are shorter than 2.65 Å, Table 4. Such short O···O distances are generally indicative of hydrogen bonding (Ichikawa, 1978; Joswig, Fuess & Ferraris, 1982), and we can conclude that a proton should be located somewhere between each of these pairs of oxygen ions. A comparison with the stoichiometry shows we have identified the correct number of proton sites (four per formula unit), as two of the O···O bonds pass through inversion centers. We can use this result to generate a distribution of protons within the structure and differentiate between sulfur and phosphorus. In one of the three XO_4 groups, all four O atoms participate in hydrogen bonds, whereas in the other two, only two O atoms form hydrogen bonds. Given the difference in valence between S^{6+} and P^{5+}, or, alternatively stated, the difference in pK values of sulfuric and phosphoric acids, we can conclude that the first XO_4 group is a phosphate and that the latter two are sulfates. A similar difference in the fraction of O atoms that participate in hydrogen bonds was observed in diammonium trihydrogenarsenate sulfate by Boubia, Averbuch-Pouchot & Durif (1985). Furthermore, stoichiometric considerations again support the conclusion as a 1:2 mole ratio of phosphorus to sulfur is required to obtain the correct chemical formula.

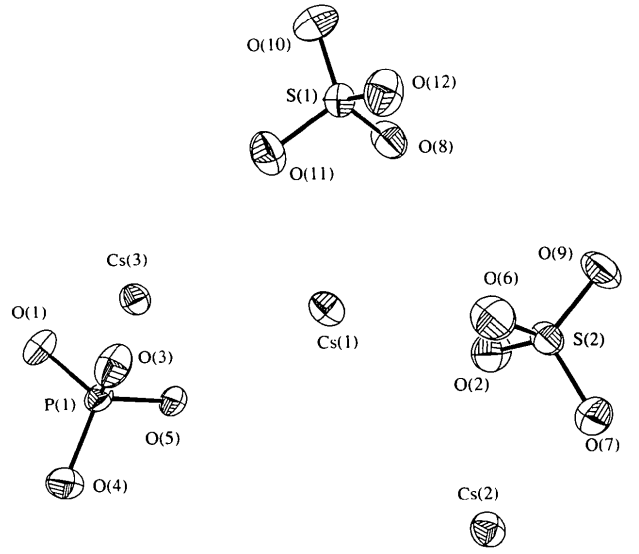

Fig. 1. A thermal ellipsoid representation of the structure of $Cs_3(HSO_4)_2(H_2PO_4)$ with an electron probability of 50%.

The hydrogen bonds in $Cs_3(HSO_4)_2(H_2PO_4)$ connect the XO_4 tetrahedra to form 'zigzag' chains that extend along (101). These are stacked in an alternating checker-board fashion with chains of face-sharing Cs polyhedra, as shown in Fig. 2. This configuration gives $Cs_3(HSO_4)_2(H_2PO_4)$, a structure which is very similar to that of the intermediate temperature form (phase II) of $CsHSO_4$ (Belushkin, David, Ibberson & Shuvalov, 1991). In fact, the former could be considered a derivative structure of the latter. In the sulfate, Cs polyhedral chains are also formed by face sharing and these are also stacked in a checker-board fashion with SO_4 anion chains. In both compounds there are equal numbers of polyhedra in the repeat units of each type of chain. The greater size of the Cs polyhedra (relative to the XO_4 tetrahedra) results in a structural 'mismatch' that is accommodated by the creation of gaps between neighboring XO_4 tetrahedra. This is shown in Fig. 3 for $Cs_3(HSO_4)_2(H_2PO_4)$. In both the sulfate and the present compound, protons are located within these gaps.

The difference between $Cs_3(HSO_4)_2(H_2PO_4)$ and II–$CsHSO_4$ lies primarily in the incorporation of PO_4 groups and excess protons into the former. In $Cs_3(HSO_4)_2(H_2PO_4)$ every third XO_4 group along the chains is a PO_4 group. The chain repeat distance in $Cs_3(HSO_4)_2(H_2PO_4)$ is consequently three times as long as in the parent structure – six polyhedra *versus* two. The additional protons that must be simultaneously incorporated for charge balance reasons reside in gaps between PO_4 tetrahedra that exist in the direction normal to $[10\bar{1}]$ and in the (010) plane. These gaps are more difficult to discern in the actual structure than the gaps that exist along the chains (described above), but can be visualized from the schematic provided in Fig. 2.

The cross-linking between chains gives rise to a three-dimensional sulfate–phosphate structure as shown in Fig. 4.

The relationship between $Cs_3(HSO_4)_2(H_2PO_4)$ and II–$CsHSO_4$ is very similar to that between the room-temperature forms of $CsHSO_4$ [a chain structure (Itoh, Ukeda, Ozaki & Nakamura, 1990)] and CsH_2PO_4 [a layered structure (Matsunaga, Itoh & Nakamura, 1980)]. The phosphate can be considered a derivative structure of the sulfate, in which all the SO_4 groups have been replaced with PO_4 groups and charge balance is achieved by introducing excess protons. As in the earlier relationship, the one-dimensional chains found in the parent structure are interconnected by hydrogen bonds in the derivative structure, and, in this case, give rise to two-dimensional layers. The analogy in the relationships is significant not only for purely crystal-chemical reasons, but also of possible implications in synthetic chemistry. It may be possible that, by simply varying the S/P ratio, compounds can be tailored to maintain a desired structure, in terms of Cs polyhedra and anion tetrahedra, and simultaneously to exhibit a desirable dimensionality in the hydrogen-bonding scheme.

Because $Cs_3(HSO_4)_2(H_2PO_4)$ is of interest for its electrical properties, it is important to examine the possibility of contributions to the observed conductivity from Cs^+ ion migration. The chains of polyhedra in which the cesium ions reside exhibit a feature often conducive to fast ion transport, that is, they share faces. In the present compound, however, the interconnecting faces are much too small to accommodate Cs^+ ion migration. For example, assuming O atoms to have the usual ionic radius of 1.4 Å (Shannon & Prewitt, 1969), the O(7)—O(11)—O(2) face shared by the Cs(1) and Cs(2) polyhedra could be expected to permit comfortable passage of only ions 1.1 Å in radius or smaller. Furthermore, in order to exhibit Cs^+ conduction, interstitial sites large enough to accommodate the ion, for at least short periods of time, must exist within the structure. Because of the rather dense packing of the Cs polyhedra in $Cs_3(HSO_4)_2(H_2PO_4)$, no such sites exist. We can safely assume, therefore, that Cs^+ does not contribute to the conductivity of $Cs_3(HSO_4)_2(H_2PO_4)$ while in this room-temperature form.

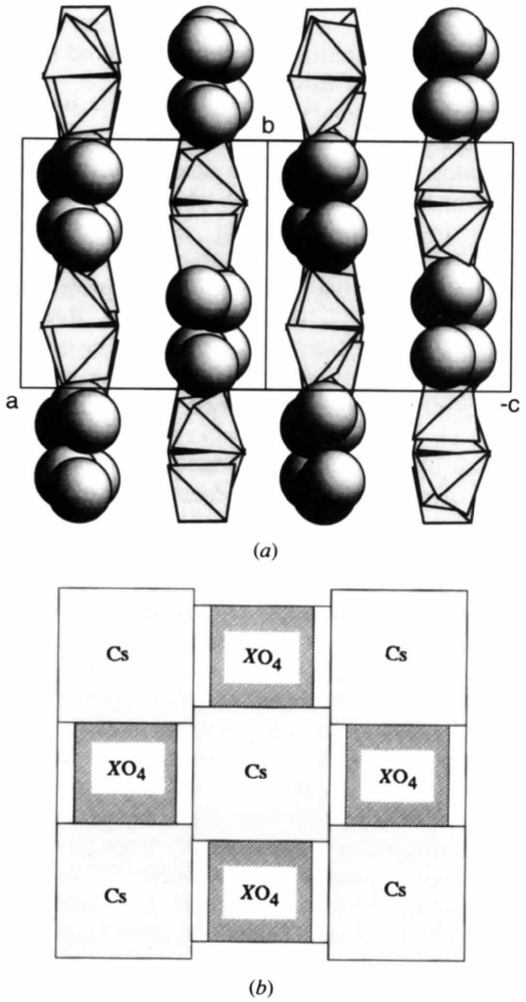

Fig. 2. The structure of $Cs_3(HSO_4)_2(H_2PO_4)$ projected along (101). (*a*) XO_4 groups are shown as tetrahedra, whereas Cs atoms are shown simply as spheres for clarity; (*b*) scheme of the structure emphasizing the checker-board motif.

Hydrogen bonding

A wealth of data concerning hydrogen-bonding, particularly in solid acid phosphates and sulfates, has been gathered and analyzed by numerous authors (Catti, Ferraris & Ivaldi, 1979; Ichikawa, 1986). The results of these analyses permit a more precise identification of proton positions in $Cs_3(HSO_4)_2(H_2PO_4)$. In Fig. 5 we

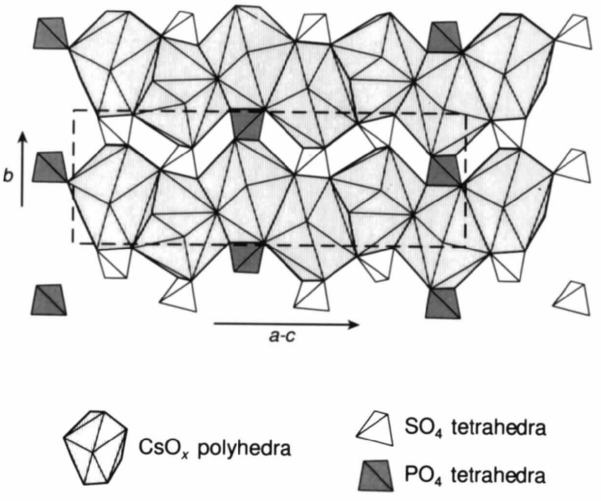

Fig. 3. The structure of $Cs_3(HSO_4)_2(H_2PO_4)$ viewed with the (101) form in the plane of the paper. Notice the gaps between neighboring XO_4 tetrahedra.

plot the linear regression lines describing the correlation between X—OH and O···O distances, as obtained by Catti, Ferraris & Ivaldi (1979) for sulfates, and by Ichikawa (1986) for phosphates. In the work of Ichikawa, PO_4 groups were differentiated on the basis of the number of hydrogen bonds they formed. Unfortunately, no saturated PO_4 groups – ones in which all four O atoms are hydrogen bonded – such as that found in $Cs_3(HSO_4)_2(H_2PO_4)$, were included in Ichikawa's study. Fig. 5, therefore, shows data for phosphate tetrahedra with only two O atoms which are hydrogen-bonded. In the more limited study by Catti, Ferraris & Ivaldi, no distinction was made between sulfate groups with differing numbers of hydrogen bonds, and thus the regression line presumably includes data from all types of SO_4 groups. In addition to these two curves, Fig. 5 also provides data for the room- and mid-temperature structures of $CsHSO_4$ (Belushkin, David, Ibberson & Shuvalov, 1991; Itoh, Ukeda, Ozaki & Nakamura, 1990, respectively) and that of CsH_2PO_4 (Matsunaga, Itoh & Nakamura, 1980).

It is well known that X—OH distances are, in general, longer than X—O distances; this is clearly evident for S—O and P—O bonds from Fig. 5. Consequently, it is possible to use differences in bond lengths to identify with which O in the O···O bond the proton is more highly associated. The H(1) proton, for example, which bonds O(4) and O(7), is surely located in the vicinity of the O(4) atom, as the P—O(4) bond distance is significantly greater than the S—O(7) distance. Similarly, on the basis of S(2)—O(6) and S(1)—O(11) bond distances, we can determine that the H(2) proton, which bonds O(6) with O(11), is likely to be closer to O(6) than O(11). The difference between the two X—O bond distances P—O(3) and S(1)—O(8), associated with the H(3) proton, is rather small, however, we can still conclude that the proton is more likely located in the vicinity of O(3).

These observations raise an important point in the hydrogen-bonding geometry of $Cs_3(HSO_4)_2(H_2PO_4)$: as the O···O distance decreases, the difference between the two X—O distances also decreases. This indicates that the proton becomes more centrally located as the two O atoms it bonds approach one another. This is in general agreement with the findings of Ichikawa (1986). In the case of the two remaining protons, H(4) and H(5), the O···O distances are quite small. Furthermore, the data points [O(1)···O(1) *versus* P—O(1) and O(5)···O(5) *versus* P—O(5)] coincide almost precisely with the points obtained in CsH_2PO_4 for P—O bonds involved in disordered, symmetric hydrogen bonds. These two observations strongly suggest that the interphosphate

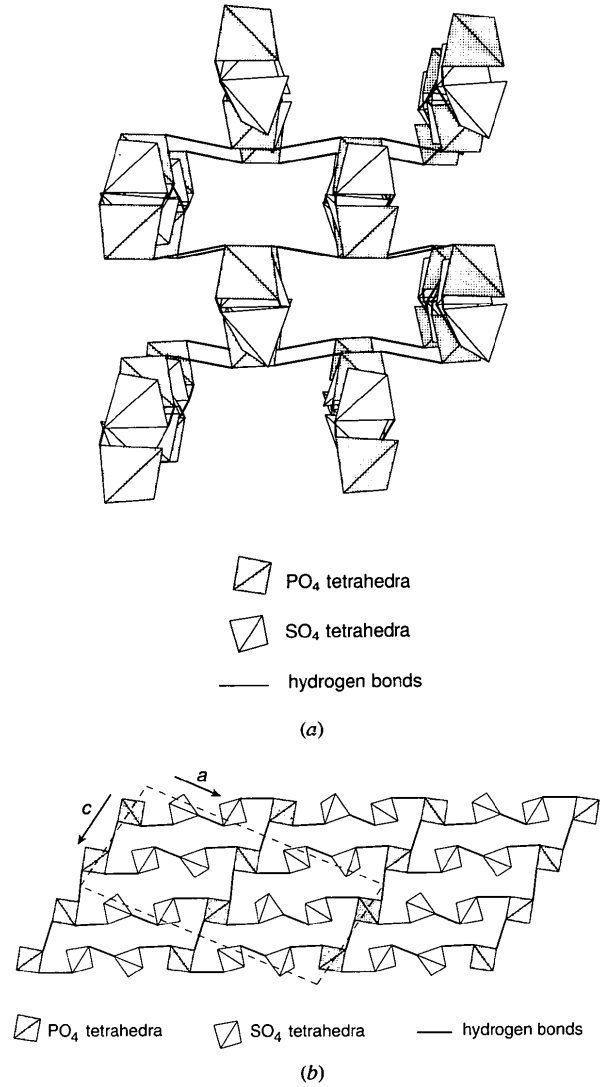

Fig. 4. The arrangement of XO_4 tetrahedra in $Cs_3(HSO_4)_2(H_2PO_4)$ and the hydrogen bonds between them: (*a*) along (101); (*b*) along (010).

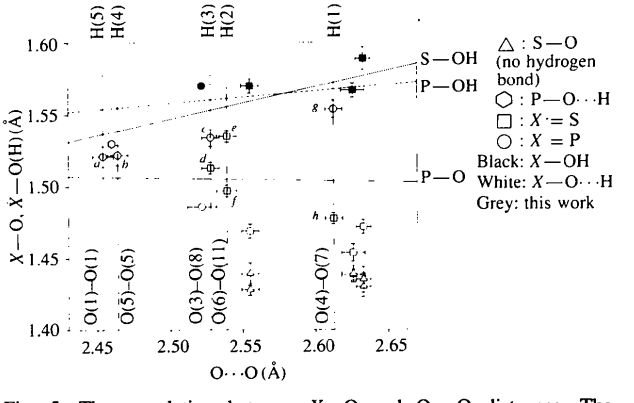

Fig. 5. The correlation between X—O and O···O distances. The curve showing S—OH data is from Catti, Ferraris & Ivaldi (1979), whereas those for P—OH and P—O are from Ichikawa (1986). The points labeled with letters represent the present work: (*a*) P—O(1); (*b*) P—O(5); (*c*) P—O(3); (*d*) S(1)—O(8); (*e*) S(2)—O(6); (*f*) S(1)—O(11); (*g*) P—O(4); (*h*) S(2)—O(7).

hydrogen bonds in the present structure are also disordered and, because of the presence of an inversion center, are symmetric.*

In summary, there are three protons located in fully occupied sites that give rise to XO_4 chains (or rather ┼(PO$_4$)—(SO$_4$)—(SO$_4$)┼) along (101). Two additional protons are located in disordered, symmetric sites and connect the chains into a three-dimensional structure. The arrangement of short (—), long (···) and disordered (·-·) H—O bonds is shown schematically below.

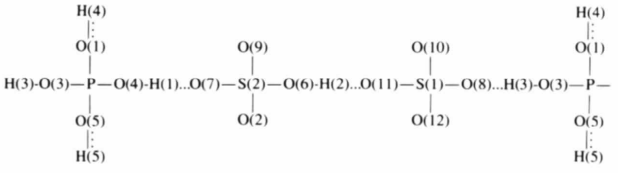

Phase transitions

As reported in our earlier work, $Cs_3(HSO_4)_2(H_2PO_4)$ undergoes a superprotonic phase transition in the temperature range 381–398 K, showing a sudden increase in its conductivity by two orders of magnitude (Haile, Lentz, Kreuer & Maier, 1995). High-temperature Guinier film data clearly show transitions both on heating and cooling (Fig. 6). Both the conductivity measurements and the X-ray powder diffraction data indicate that, upon cooling, the compound remains in the superprotonic phase to temperatures well below that of the initial transition. The differential scanning calorimetry data, Fig. 7, on the other hand, show, upon heating, a very weak but reproducible peak at 383 K and a first-order transition at 418 K. No transitions were evident upon cooling. The transition detected at 418 K is more likely to correspond to the structural transformation between the monoclinic phase and the superprotonic phase rather than to thermal decomposition. Water loss, as determined from TGA/mass spectroscopy experiments, occurs in $Cs_3(HSO_4)_2(H_2PO_4)$ at temperatures between 423 and 553 K (Fig. 8), with maximum weight loss occurring at approximately 483 K. The differences between the results from conductivity and diffraction experiments and from differential scanning calorimetry might possibly be explained by differences in heating rates. Samples used for conductivity and diffraction measurements were heated rather slowly, *ca* 10 K h^{-1}, in order to ensure equilibration. Differential scanning calorimetry, on the other hand, was performed at 5 and 10 K min^{-1}, in order to ensure that the transition would be detectable. This faster heating rate may have enabled the low-temperature phase to exist in a metastable state at temperatures above the superprotonic transition. The very weak DSC peak observed at 383 K might reflect the loss of surface-absorbed water.

The powder diffraction peaks of the high-temperature phase can be indexed on the basis of a body-centered cubic (BCC) lattice with a lattice constant of 6.961 (12) Å (as averaged over many patterns). However, the unit cell is more likely rhombohedral with $\alpha \simeq 90°$. The cell has a volume of 337 Å^3, suggesting a value of $Z = 1$, from which one calculates a density of 3.41 Mg m^{-3}. One formula unit per unit cell translates into three Cs atoms per unit cell, an impossible number to obtain in a BCC cell without the introduction of partial occupancies, but one that is easily accommodated in a rhombohedral cell.

In addition to a superprotonic transition and decomposition at elevated temperatures, many solid acid sulfates and phosphates exhibit ferroelectric transitions at depressed temperatures. Given the probable presence of two disordered protons in $Cs_3(HSO_4)_2(H_2PO_4)$, the present compound is very likely to undergo such a transition. Ichikawa has attempted to correlate ferroelectric transition temperatures with O···O

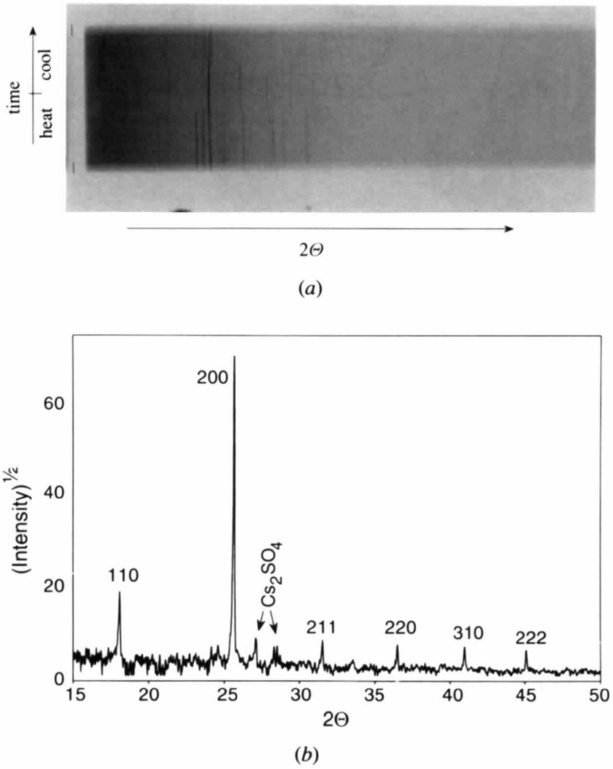

Fig. 6. X-ray powder diffraction data for $Cs_3(HSO_4)_2(H_2PO_4)$. (*a*) Film data showing transitions upon cooling and heating; (*b*) scanned and calibrated intensities at 413 K with peaks indexed according to a rhombohedral (psuedo-body-centered cubic) cell.

* Of course, it is structures which generate symmetry elements rather than symmetries which constrain structures. Ignoring quantum effects, at any particular 'instant' and in any particular bond, the proton must be located on one side or the other of the inversion center, thereby disturbing the local symmetry. Thus, the observation of dynamic and/or structural disorder within a symmetric, double-minima potential well is restricted to the extended time and length scales of the diffraction event.

distances in various classes of compounds, differentiated by the dimensionality of the disordered hydrogen-bond network (ordered hydrogen bonds are ignored). The connectivity between PO_4–H–H′–PO_4 along the direction normal to (001) gives rise to a one-dimensional network in $Cs_3(HSO_4)_2(H_2PO_4)$. From Fig. 4 in Ichikawa, Gustafsson & Olovsson (1994) one can predict that the present compound will have a ferroelectric transition at 125 K. Low-temperature dielectric measurements of $Cs_3(HSO_4)_2(H_2PO_4)$ can provide data for either suppporting or refuting the conclusions of the aforementioned authors.

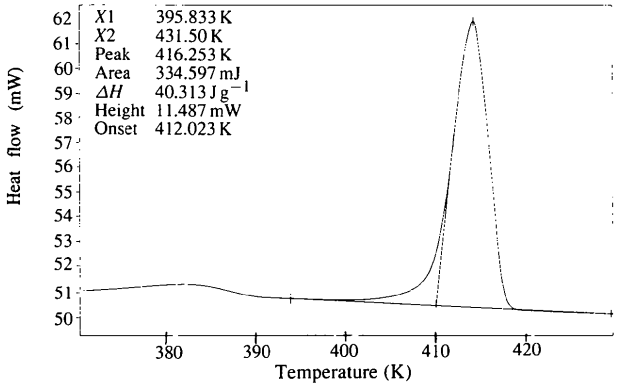

Fig. 7. Differential scanning calorimetry (DSC) measurement of $Cs_3(HSO_4)_2(H_2PO_4)$.

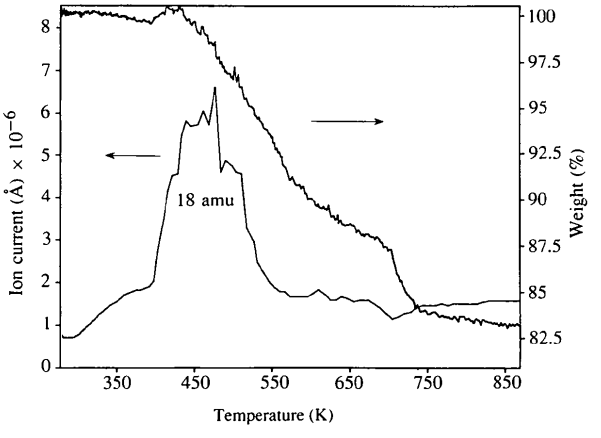

Fig. 8. Weight loss as a function of temperature in $Cs_3(HSO_4)_2(H_2PO_4)$.

Many colleagues have kindly donated their time and expertise to this work. Of those at MPI, we thank, in particular, Gisela Lentz for growing the crystals, Herr Karl Peters for providing single-crystal intensity data and Herr Willie Rötenbach for performing the high-temperature powder diffraction. Frau Ortrud Buresch performed the ICP spectroscopy, and Frau Claudia Winckler conducted the SEM imaging and microprobe analyses. We gratefully acknowledge Dr Quintinn Johnson of MDI, who scanned in the powder film data and David McCready of PNL, who aided in the powder data analysis. This work was supported, in part, by the Alexander von Humboldt Foundation and by Battelle National Laboratories.

References

BARANOV, A. I., FEDOSYUK, R. M., SCHAGINA (*sic*), N. M. & SHUVALOV, L. A. (1984). *Ferroelectr. Lett.* **2**, 25–28.

BELUSHKIN, A. V., DAVID, W. I. F., IBBERSON, R. M. & SHUVALOV, L. A. (1991). *Acta Cryst.* B**47**, 161–166.

BOUBIA, M., AVERBUCH-POUCHOT, M. T. & DURIF, A. (1985). *Acta Cryst.* C**41**, 1562–1564.

CATTI, M., FERRARIS, G. & IVALDI, G. (1979). *Acta Cryst.* B**35**, 525–529.

CROMER, D. T. & WABER, J. T. (1974). *International Tables for X-ray Crystallography*, Vol. IV, Table 2.2A, pp. 128–134. Birmingham: Kynoch Press. (Present distributor Kluwer Academic Publishers, Dordrecht.)

HAILE, S., LENTZ, G., KREUER, K.-D. & MAIER, J. (1995). *Solid State Ionics*, **77**, 128–134.

ICHIKAWA, M. (1978). *Acta Cryst.* B**34**, 2074–2080.

ICHIKAWA, M. (1986). *Acta Cryst.* B**43**, 23–38.

ICHIKAWA, M., GUSTAFSSON, T. & OLOVSSON, I. (1994). *J. Mol. Struct.* **321**, 21–33.

ITOH, K., UKEDA, T., OZAKI, T. & NAKAMURA, E. (1990). *Acta Cryst.* C**46**, 358–361.

JOHNSON, C. K. (1971). *ORTEP*II. Report ORNL-3794, revised. Oak Ridge National Laboratory, Tennessee, USA.

JOSWIG, W., FUESS, H. H. & FERRARIS, G. (1982). *Acta Cryst.* B**38**, 2798–2801.

MATSUNAGA, H., ITOH, K. & NAKAMURA, E. (1980). *J. Phys. Soc. Jpn*, **48**, 2011–2014.

MERINOV, B. V., BARANOV, A. I., SHUVALOV, L. A. & SHCHAGINA, N. M. (1991*a*). *Sov. Phys. Cryst.* **36**, 321–324.

MERINOV, B. V., BARANOV, A. I., SHUVALOV, L. A. & SHCHAGINA, N. M. (1991*b*). *Kristallografiya*, **36**, 584–590.

PAWLACZYK, CZ., SALMAN, F. E., PAWLOWSKI, A., CZAPLA, Z. & PIETRASZKO, A. (1986). *Phase Transit.* **8**, 9–16.

PAWLOWSKI, A., PAWLACZYK, CZ. & HILCZER, B. (1990). *Solid State Ionics*, **44**, 17–19.

SHANNON, R. D. & PREWITT, C. T. (1969). *Acta Cryst.* B**25**, 925–946.

SHELDRICK, G. M. (1985). In *Crystallographic Computing* 5, edited by D. MORAS, A. D. PODJARNY & J. C. THIERRY, pp. 145–157. Oxford Univ. Press.

SHELDRICK, G. M. (1992). In *Crystallographic Computing* 3, edited by G. M. SHELDRICK, C. KRÜGER & R. GODDARD, pp. 175–189. Oxford Univ. Press.

SIMON, V. A. (1971). *J. Appl. Cryst.* **4**, 138–145.